Title

Visual Experience Influences Dendritic Orientation but Is Not Required for Asymmetric Wiring of the Retinal Direction Selective Circuit

Journal

Cell Reports, 31(13)

ISSN

2639-1856

Authors

El-Quessny, Malak
Maanum, Kayla
Feller, Marla B

Publication Date

2020-06-01

DOI

10.1016/j.celrep.2020.107844

Peer reviewed

HHS Public Access

Author manuscript

Cell Rep. Author manuscript; available in PMC 2020 July 21.

Published in final edited form as:

Cell Rep. 2020 June 30; 31(13): 107844. doi:10.1016/j.celrep.2020.107844.

Visual Experience Influences Dendritic Orientation but Is Not Required for Asymmetric Wiring of the Retinal Direction Selective Circuit

Malak El-Quessny[1], **Kayla Maanum**[2], **Marla B. Feller**[1,3,4,*]

[1]Helen Wills Neuroscience Institute, University of California, Berkeley, Berkeley, CA 94720, USA

[2]Department of Integrative Biology, University of California, Berkeley, Berkeley, CA 94720, USA

[3]Department of Molecular and Cell Biology, University of California, Berkeley, Berkeley, CA 94720, USA

[4]Lead Contact

SUMMARY

Changes in dendritic morphology in response to activity have long been thought to be a critical component of how neural circuits develop to properly encode sensory information. Ventral-preferring direction-selective ganglion cells (vDSGCs) have asymmetric dendrites oriented along their preferred direction, and this has been hypothesized to play a critical role in their tuning. Here we report the surprising result that visual experience is critical for the alignment of vDSGC dendrites to their preferred direction. Interestingly, vDSGCs in dark-reared mice lose their inhibition-independent dendritic contribution to direction-selective tuning while maintaining asymmetric inhibitory input. These data indicate that different mechanisms of a cell's computational abilities can be constructed over development through divergent mechanisms.

Graphical Abstract

*Correspondence: mfeller@berkeley.edu.

AUTHOR CONTRIBUTIONS

M.Q. conducted the experiments and analyzed all the data. K.M. conducted mosaic analysis experiments and measured dendritic field size. M.Q. and M.B.F. designed the experiments and wrote the manuscript.

SUPPLEMENTAL INFORMATION

Supplemental Information can be found online at https://doi.org/10.1016/j.celrep.2020.107844.

DECLARATION OF INTERESTS

The authors declare no competing interests.

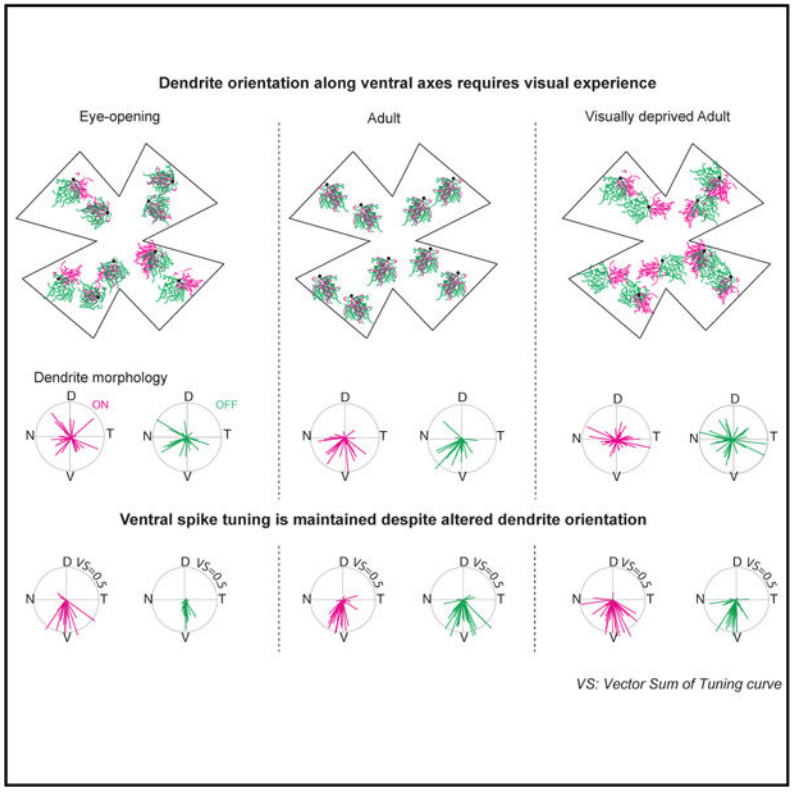

In Brief

El-Quessny et al. investigate the structure-function relationship of a ventrally-tuned directionally-selective ganglion cell (vDSGC), which has ventrally oriented dendrites during adulthood. They find that visual experience orients the vDSGC dendrites ventrally, affecting dendritic mechanisms, while sparing circuit mechanisms, for direction computations.

INTRODUCTION

Neural computations rely upon precise wiring, which emerges during development. A classic example of such a computation is direction selectivity. In the retina, direction-selective ganglion cells (DSGCs) fire many action potentials in response to stimuli moving in a preferred direction (PD) and few to no action potentials in response to stimuli moving in the opposite or null direction (ND) (Barlow and Levick, 1965). The direction-selective (DS) computation is based primarily on the asymmetric wiring of an inhibitory interneuron, the starburst amacrine cell (SAC), onto DSGCs such that motion in a DSGC's ND generates more inhibition than motion in the PD (Vaney and Taylor, 2002; Demb, 2007). This asymmetric wiring is present as early as postnatal day 10 (P10), a few days prior to eye opening (Wei et al., 2011; Yonehara et al., 2011), and is a consequence of DSGCs' preferentially forming synapses with SACs located on their null side, relative to their preferred side (Morrie and Feller, 2015).

What instructs this asymmetric wiring? The establishment of wiring specificity in the nervous system is a complex process involving an interplay between molecular cues dictating synaptic specificity and activity-dependent synaptic strengthening or weakening (Leighton and Lohmann, 2016). In addition, it is thought that form instructs function, i.e., that the morphology of axons and dendrites and their relative spatial organization dictate the location of synapses (Wong and Ghosh, 2002; Richards and Van Hooser, 2018). In the retinal DS circuit, the relative roles of molecular specification, neural activity, and the spatial organization of presynaptic (SAC) relative to postsynaptic (DSGC) cells in instructing this wiring remains a mystery.

A few studies have assessed the role of SAC morphology in instructing asymmetric wiring. SACs have radially symmetric processes and serial electron microscopy (EM) reconstructions show that the orientation of individual SAC process is tightly correlated with the ND of the DSGCs that receive synaptic input from them (Briggman et al., 2011; Ding et al., 2016; Bae et al., 2018). SAC-specific genetic deletion of the cell-adhesion protein protocadherin G (Pcdhg) (Lefebvre et al., 2012; Kostadinov and Sanes, 2015) or the axon guidance protein semaphorin 6A (Sema6A) (Sun et al., 2013), both of which alter SAC radial morphology, eliminating directional tuning of DSGCs. However, in the case of Sema6A, loss of DS is due to a reduction in asymmetric inhibition while asymmetric wiring is maintained (Morrie and Feller, 2018). Interestingly, a hypo-morphic mutation in the FRMD7 gene, which is associated with congenital nystagmus in humans, abolishes direction selectivity along the horizontal axis without affecting SAC morphology (Yonehara et al., 2016). The mechanism by which FRMD7 or other molecules expressed by SACs instruct the selective wiring to different subtypes of DSGCs remains unknown.

An alternative hypothesis is that the postsynaptic DSGC dendrites influence asymmetric wiring. DSGCs that encode motion in different directions have distinct molecular profiles and morphological characteristics (Kay et al., 2011; Trenholm et al., 2011). Across the nervous system, the shape of a dendrite has implications for the organization of synaptic inputs as well as its functional role within a circuit (Wong and Ghosh, 2002; Richards and Van Hooser, 2018). Indeed, a recent study indicated that the relative orientation of dendrites and axons were more important than molecular identity in instructing synapse specificity in spinal cord sensory motor circuits (Balaskas et al., 2019).

One way to investigate the role of DSGC morphology in the wiring of DS circuits would be to alter the morphology of the DSGC and assess its consequences on DS tuning and synaptic wiring. To do this, we used the Hb9-GFP mouse line, which expresses GFP in a subset of ON-OFF ventral-preferring DSGCs (vDSGCs). Uniquely among DSGCs, vDSGCs' dendritic fields are asymmetric and oriented in their PDs (Trenholm et al., 2011; Sabbah et al., 2017), making them more likely to form synapses with SACs on their null side, a hypothesis based on serial EM reconstructions of SAC and DSGC dendrites (Briggman et al., 2011). We found that in mice that were dark-reared (DR) from birth to adulthood, dendrites of vDSGCs were not preferentially oriented toward the ventral direction. Although dark-rearing prevented the establishment of inhibition-independent direction selectivity, these dramatic changes in dendritic morphology did not alter the asymmetric wiring of inhibition or alter the overall vDSGCs direction selectivity.

RESULTS

Asymmetric Dendrites of vDSGCs Are Dispersed at Eye Opening and in Dark-Reared Adults

Dark-rearing had a dramatic impact on the dendritic organization of vDSGCs. To characterize the impact of dark-rearing on the dendritic morphology of vDSGCs, we filled Hb9-GFP+ cells in retinas dissected from normally reared (NR; 12 h dark/light cycle) and dark-reared (DR;24 h dark) adult mice and from mice that had just opened their eyes (P13/P14; 12 h dark/light cycle) (Figure 1A). Dendritic morphology was independently characterized for ON and OFF arbors by a vector pointing from the soma to the dendritic center of mass (dCOM), whose magnitude (r) corresponded to the degree of dendritic asymmetry and whose angle (W) corresponded to dendritic orientation (Figure S1; STAR Methods).

As described previously (Trenholm et al., 2011), NR adult vDSGC dendrites were asymmetric, and both ON and OFF dendrites were oriented ventrally (Figures 1A and 1B). NR adult vDSGC ON and OFF dendrites were oriented ventrally and within 45° of each other (Figures 1A and 1B). At P13/P14, vDSGC ON and OFF dendrites were asymmetric (Figure 1C), but they were not preferentially oriented toward the ventral direction (Figure 1D) and displayed some variability in their alignment with each other (Figure 1E). Surprisingly, in mice that were DR, the orientations of vDSGCs' ON and OFF dendrites were similar to the eye opening distribution, asymmetric (Figure 1C), and their orientation deviated significantly from the ventral direction (Figures 1D and S1; Table S1). Hence, visual experience is necessary for the alignment of ON and OFF vDSGC dendrites to the ventral axis of the retina.

We also examined other features of vDSGC dendrites after dark-rearing. First, we found that dark-rearing increased the dendritic field size of OFF-stratifying dendrites (Figure 1F), similar to the impact of dark-rearing on OFF-stratifying asymmetric J-RGCs (Elias et al., 2018). Second, dark-rearing had no impact on mosaic organization of vDSGCs (Figure S2), indicating that their spacing may not be set by homotypic interactions between dendritic segments (Rockhill et al., 2000; Kay et al., 2012).

One unique property of vDSGCs among DSGCs is that they are gap junction coupled and have been shown to retain their gap junction coupling into adulthood (Trenholm et al., 2013). Coupling broadens their directional tuning at low/scotopic light levels (Yao et al., 2018). Recent data indicate that the extent of coupling is influenced by visual experience (Zhang et al., 2020). To address whether dark-rearing influences vDSGC coupling in adulthood, we conducted tracer coupling experiments on NR and DR adult vDSGCs (Figure S3A). In dark-reared mice, the pattern of tracer-coupled vDSGCs did not change relative to NR mice (Figure S3B). Interestingly, DR mice showed a small but significant increase in the number of tracer-coupled cells (Figures S3C and S3D), though the proportion of GFP+ cells to which they were coupled did not change (Figure S3E). Hence, changes in coupling between vDSGCs are not likely to mediate the increased variability of dendritic orientation in DR mice.

Ventral Motion Preference Is Preserved in Dark-Reared vDSGCs Despite Altered Dendritic Morphology

Does function follow form? In NR mice, vDSGC dendrites are oriented in the same direction as their motion preference. This orientation potentially influences at least two different mechanisms that contribute to their DS computation. First, DSGCs receive stronger ND inhibition from SACs located on the null side of the DSGC soma (Briggman et al., 2011; Morrie and Feller, 2015; Ding et al., 2016; Bae et al., 2018). For vDSGCs, this preferential wiring is potentially facilitated by the ventral orientation of their dendrites. Second, unlike other DSGCs, vDSGCs retain some directional tuning in the absence of inhibitory input (Trenholm et al., 2011), a feature attributed to their asymmetric dendrites.

To determine the impact of development and visual experience on DS tuning of vDSGCs, we conducted cell-attached recordings of spikes in response to drifting bars moving in eight different directions in NR adult and P13/P14 as well as DR adult animals (Figure 2A). Surprisingly, we observed no differences in the strength of DS tuning in any of the experimental groups (Figure 2B; Table S2). Note that OFF responses were less tuned at eye opening (Figure 2C), consistent with findings that OFF DS circuits mature later than ON circuits (Hoon et al., 2014; Rosa et al., 2016). Thus, we only analyzed ON spike tuning for P13/P14. We found a significant increase in the variance of the PD of spiking relative to the ventral axis (PDΔv) for OFF responses (Figure S4B), similar to what was observed using population imaging of direct selective responses (Bos et al., 2016). Note a direct comparison with this previous study (Bos et al., 2016) is not possible, because the responses of Hb9-GFP cells, which constitute only a subset of vDSGCs (Sabbah et al., 2017), were not analyzed separately.

The preservation of ventral motion preference in P13/P14 and adult DR vDSGCs (Figures 2D and S4A) resulted in a strong dissociation of dendritic orientation ($dCOM_{\Theta}$) and spiking PD (PD_{Θ}) (Figure 2D). Moreover, there was no correlation between the relative dendritic orientation and the PD ($|dCOM_{\Theta}\text{-}PD_{\Theta}|$) with the tuning of the spike responses (Figures 2D and S4). Hence, DS tuning of vDSGCs appears to be independent of the orientation of the dendrites.

Dendritic Alignment Is Critical for Inhibition-Independent Tuning of vDSGCs

The asymmetric morphology of vDSGCs, along with the alignment of their dendritic arbor and PD, has been postulated to underlie their ability to retain some directional tuning in the absence of inhibitory input (Trenholm et al., 2011). Modeling experiments suggest that this postsynaptic mechanism of directional tuning is mediated by nonlinear conductances at the distal dendrites of vDSGCs, which allow them to integrate excitatory input along the ventral or centrifugal direction (soma to dendrite) more efficiently than in the dorsal or centripetal direction (dendrite to soma) (Trenholm et al, 2011; 2013). However, the relationship between dendritic orientation and postsynaptic, inhibition-independent mechanisms of directional tuning has not been fully explored.

To establish whether there is a correlation between dendritic morphology and inhibition-independent tuning, we conducted both cell-attached and current-clamp recordings from

vDSGCs in NR adults in the presence of a $GABA_A$ receptor blocker, gabazine (50 μM) (Figure 3A). For these experiments, we used slower stimulation velocities to enhance the postsynaptic contributions to directional tuning (Trenholm et al., 2011). Consistent with previous findings, both ON and OFF responses retained some of their directional tuning in the absence of inhibitory input (Figures 3C and S5C). Interestingly, the direction of ON tuning deviated from the ventral axis (Figure 3c; Figure S5E; Table S2).

We observed a significant decrease in both ON and OFF inhibition-independent tuning in vDSGCs recorded from DR mice as measured by the vector sum (Figures 3B and 3C; Figure S5D), though this difference did not reach statistical significance when comparing direction selectivity index (DSI) across rearing conditions. Note that given the large amount of spiking of DSGCS in the presence of gabazine, the vector sum was a less variable measure of tuning. Hence, visual experience is critical for the maturation of the inhibition-independent mechanism of direction selectivity. We postulate that because this reduction in inhibition-independent tuning is not associated with a loss of dendritic asymmetry, dark-rearing may disrupt the location and or strength of the nonlinearity that underlies the dendritic computation of direction selectivity.

This result led us to explore the relationship between dendritic morphology and inhibition-independent tuning on a cell-by-cell basis in normally reared mice. The strength of the tuning of both ON and OFF responses was only weakly correlated with the magnitude of dendritic asymmetry (Figure S5F). However, we observed a correlation between the relative alignment of the OFF dendrite and OFF PD ($|dCOM_\Theta\text{-}PD_\Theta|$) with the strength of tuning (Figures 3D and S5E, right), though this correlation was lacking for ON responses (Figure 3D; Figure S5E, left). These data indicate that ON and OFF dendrites of vDSGCs may use different mechanisms of synaptic integration. Hence, in NR animals, dendritic alignment along the ventral axis influences the contribution of inhibition-independent tuning to the overall directional tuning of the cell, specifically for the OFF pathway.

Asymmetric Inhibition from Null Side Starburst Cells Is Preserved in Dark-Reared vDSGCs Despite Altered Dendritic Morphology

Since ventral motion preference is preserved in DR vDSGCs, we assessed the impact of dark-rearing on the directional tuning of both inhibitory (Figure 4; Table S3) and excitatory (Figure S6) synaptic inputs using the whole-cell voltage-clamp technique. Inhibitory synaptic input was highest for dorsal motion (Figures 4A and 4B) and had similar directional tuning strength (Figure 4C) and tuning angle deviation from the dorsal axis (Figure 4D) in vDSGCs from NR adult, P13/P14, and DR adult mice. Hence, asymmetric inhibition in response to ND motion is independent of visual experience and vDSGC dendritic orientation. In NR and DR adults, we observed small excitatory postsynaptic current (EPSC) tuning in the PD, which was absent at P13/P14 (Figure S6C).

A feature of the DS circuit in the retina is the presence of spatially offset inhibition (Fried et al., 2002; Hanson, 2019; Pei, 2015; Sivyer, 2010). This indicates that SACs located on the ventral side of the vDSGC will provide more inhibitory input (Figure 4E). To determine whether directionally tuned inhibitory postsynaptic currents (IPSCs) were generated by SACs located on the null side of vDSGCs, we mapped the excitatory and inhibitory

receptive fields of NR and DR adult vDSGCs by recording synaptic currents evoked by squares of light sequentially presented at 100 block-shuffled locations within a soma-centered grid. We calculated the vector from the soma to the center of the inhibitory and excitatory receptive fields (Figures 5A and 5B), using the magnitude (ρ) of the vector to indicate receptive field displacement, and the angle of the vector (Θ) to indicate receptive field orientation. We found that in both NR and DR adult vDSGCs, the inhibitory receptive fields were similarly oriented toward the ventral direction relative to the soma (Figure 5C). We then computed the vector from the excitatory to the inhibitory receptive field centers and observed that the magnitude of their displacement from each other was similar across rearing conditions (Figure 5D). Moreover, the angle of the vector was similarly aligned to the ventral axis ($\Delta\Theta_v$) (Figure 5E). Hence, although DR vDSGCs have displaced dendrites, they still receive spatially offset inhibition from SACs located on their null side. These data indicate that the location of dendrites does not influence their direction selectivity of the processes of their presynaptic partners (Figure 4E).

DISCUSSION

Form-function studies to date have shown that the shape of a dendrite influences its role within a circuit and that the diversity of dendritic morphologies is necessary to fulfill a wide range of neural computations (Wong and Ghosh, 2002; Lefebvre et al., 2015). This study demonstrates that the precise asymmetric wiring of synaptic circuits that mediate direction selectivity is independent of the orientation of the DSGC dendrites. Visual experience following eye opening promotes the ventral orientation of asymmetric vDSGCs, and this process is prevented by dark-rearing. Although dark-rearing reduced the inhibition-independent contribution to directional tuning, the tuning and spatial distribution of excitatory and inhibitory synaptic inputs were intact and, as a result, DR vDSGCs retained their normal directional tuning. The data presented here supports a model in which the maturation of dendritic morphology appears to be dictated by the functional circuit rather than the traditional view that dendritic morphology dictates circuit function.

Activity Influences Dendritic Morphology

We found that dark-rearing had a dramatic but specific effect on the dendrites of vDSGCs: it prevented the orientation of vDSGC dendrites in the ventral direction and, in a subset of vDSGCs, prevented the alignment of ON with OFF dendrites (Figure 1). This finding indicates that visual experience is necessary for vDSGC dendrites to orient themselves along their PD. This counters our initial hypothesis that the orientation of DSGC dendrites along their PD optimizes antiparallel wiring with null side SAC dendrites. Rather, we postulate that the orientation of the dendrites along their PD is instead necessary for the establishment of inhibition-independent mechanisms for DS.

Here we consider these findings in the context of other systems in which afferent activity plays a role in asymmetric dendritic development, including ganglion cells in the zebrafish retina (Choi et al., 2010), layer IV stellate cells in the somatosensory cortex (Woolsey and Van der Loos, 1970; Greenough and Chang, 1988; Nakazawa et al., 2018), and mitral cells of the rodent olfactory bulb (Hinds and Ruffett, 1973; Blanchart et al., 2006), among others

(for a review, see Wong and Ghosh, 2002). In developing zebrafish, retinal ganglion cells (RGCs) initially have both apical and basal dendrites pointing both toward and away from the inner plexiform layer. Upon contact with bipolar cells, RGCs' basal dendrites reorient toward the apical side to form functional synapses (Choi et al., 2010). In the heart-and-soul (*has*) mutant zebrafish, RGCs are displaced to the other side of bipolar cells, leading to an increase in basal orientation. This indicates that the location of the RGC dendrites relative to bipolar cell afferents instructs their orientation. In layer IV spiny stellate neurons in barrel cortex, activity-dependent pruning eliminates inactive dendrites oriented away from barrel centers while sparing active dendrites oriented toward the barrel center, which elaborate and stabilize (Harris and Woolsey, 1981; Narboux-Nême et al., 2012; Li et al., 2013). When thalamocortical axon input is silenced via infraorbital nerve cut, or via postsynaptic NMDA receptor knockout, spiny stellate neuron dendrites misalign with respect to barrel centers (Mizuno et al., 2014, 2018). This suggests that dendrites are oriented toward afferent activity.

Sensory experience may be required for the establishment of dendritic orientation through mechanisms that influence gene transcription. *In situ* hybridization revealed that the transcription factor BTBD3 is highly localized to the barrels of somatosensory cortex during development and that activity-dependent nuclear translocation of BTBD3 is required for the orientation of stellate neuron dendrites toward the barrel hollows. Similarly, BTBD3 is implicated in the orientation of dendrites in ferret visual cortex toward the center of ocular dominance columns whereby monocular enucleation and BTBD3 short hairpin RNA (shRNA) knockdown lead to misorientation of layer IV excitatory neuron dendrites (Matsui et al., 2013).

How does visual experience instruct vDSGCs to orient toward their PD? One possibility is that bipolar cell inputs on the preferred side are stronger and therefore dendrites on the preferred side are stabilized while dendrites on the non-preferred side are pruned. Such asymmetric wiring of bipolar cells was recently reported in ON DSGCs (Matsumoto et al., 2019). However, serial EM reconstructions of symmetric ON-OFF DSGCs (Ding et al., 2016) do not indicate such a bias, though this reconstruction has not been conducted for vDSGCs.

Another clue comes from understanding the specific aspects of visual experience that might influence the DS network. First, trained visual experience paradigms, in which animals experience only upward (PD) motion, lead to increased gap junctional coupling of vDSGCs and synchronize population spike responses (Zhang et al., 2020). ND training had no effect on coupling, and neither did changing contrast, luminance, and temporal frequency regimes of the training stimulus. Second, gap junction networks between vDSGCs are hypothesized to enable motion detection at scotopic light levels and motion discrimination at high light levels (Yao et al., 2018). Although we find that gap junction coupling between vDSGCs is un-changed in DR animals (Figure S3), this suggests that structured visual experience and synchronized network function, provided by sequential activation of gap junction networks and presynaptic inputs, may play a key role in mediating the orientation of vDSGC dendrites toward their PD.

Our finding that dark-rearing did not affect stratification differs from previous studies in which visual deprivation prevented the stratification of some ganglion cell dendrites (Tian and Copenhagen, 2001) through a process dependent on brain-derived neurotrophic factor (BDNF) activation of TrkC receptors (Liu et al., 2007). Interestingly, this activity-dependent stratification does not appear to be dictated by glutamate release from bipolar cells, as vDSGC ON dendrite stratification has been shown to rely on the expression of the adhesion molecule contactin 5 and its co-receptor Caspr4 for proper stratification, which is expressed by ON SACs (Peng et al., 2017), and stratification was normal in mice lacking release from ON bipolar cells (Kerschensteiner et al., 2009).

Implications for Postsynaptic, Inhibition-Independent Contributions to DS

Thus far, vDSGCs are the only DSGC subtype to exhibit directional tuning in the absence of inhibitory input (Trenholm et al., 2011). In the presence of the $GABA_A$ receptor antagonist gabazine, other subtypes of anterior and posterior preferring DSGCs lose their directional tuning (Ackert, 2009; Bos et al., 2016; Rivlin-Etzion et al., 2012; Wei et al., 2011). However, because of the correlation of dendritic orientation and PD in NR adult vDSGCs, it is postulated that they also possess postsynaptic mechanisms for encoding motion direction. Our results in NR adults are consistent with previous findings, in which vDSGCs retain some of their tuning in the absence of inhibitory input (Trenholm et al., 2011). By using a bar stimulus in our experiments, we were able to determine that both ON and OFF responses were partially retained during blockade of inhibition

Computational modeling experiments have shown that vDSGCs may possess nonlinear conductances, such as voltage-gated sodium channels, on their distal dendrites, allowing them to efficiently encode ventral motion (from soma to distal dendrites) more efficiently than dorsal motion (from dendrites to soma) (Trenholm et al., 2011). Using current-clamp recordings, we found that ON and OFF dendrites use different mechanisms for integrating excitatory input in the absence of inhibitory input (Figure 3C), in which ON dendrites may follow a more passive model of centripetal (dendrite-to-soma) integration (Rall, 1964), whereas OFF dendrites follow a more active model of centrifugal (soma-to-dendrite) integration (Stuart and Spruston, 2015). Dark-rearing significantly reduces this contribution to directional tuning. As asymmetric dendrites are maintained after dark-rearing, we hypothesize that visual experience is required for establishing the nonlinear conductance or the organization and kinetics of excitatory inputs onto DSGC dendrites (Matsumoto et al., 2019).

Hence, for DS cells, it appears that even though the primary computation is set up by an experience-independent molecular program, there can be additional computations set up by experience-dependent processes. This leads to the interesting hypothesis that the alignment of dendrites and the establishment of inhibition-independent tuning require the presence of the primary computation of directional preference.

STAR★METHODS

RESOURCE AVAILABILITY

Lead Contact—Further information and requests for resources and reagents should be directed to and will be fulfilled by the Lead Contact, Marla Feller (mfeller@berkeley.edu).

Materials Availability—This study did not generate new unique reagents.

Data and Code Availability—All datasets generated during and/or analyzed during the current study and all custom scripts and functions generated or used during the current study are available from the Lead Contact (mfeller@berkeley.edu) upon request.

EXPERIMENTAL MODEL AND SUBJECT DETAILS

Mice used in this study were aged from p13–60 and were of both sexes. Animals used in experiments had not previously been involved in other experiments or exposed to any drugs. Animal health was monitored daily and only healthy animals were used in experiments. To target ventral preferring DSGCs, we used Hb9::GFP (Arber et al., 1999) mice, which express GFP in a subset of DSGCs (Trenholm et al., 2011). Normally-reared animals were kept on a 12h:12h dark-light cycle. Dark-reared animals were kept on a 24h:0h dark-light cycle from birth until tissue collection. All experiments involved recording from 1–7 cells from at least 3 animals of either sex. All animal procedures were approved by the UC Berkeley Institutional Animal Care and Use Committee and conformed to the NIH Guide for the Care and Use of Laboratory Animals, the Public Health Service Policy, and the SfN Policy on the Use of Animals in Neuroscience Research.

METHOD DETAILS

Retina Preparation Mice were anesthetized with isoflurane and decapitated. Retinas were dissected from enucleated eyes in oxygenated (95% O2/5% CO2) Ames' media (Sigma) for light responses or ACSF (in mM, 119 NaCl, 2.5 KCl, 1.3 $MgCl_2$, 1 K2HPO_4, 26.2 NaHCO3, 11D-glucose, and 2.5 $CaCl_2$) for paired recordings. Retinal orientation was determined as described previously (Wei et al., 2010). Isolated whole retinas were micro-cut at the dorsal and ventral halves to allow flattening, with dorsal and ventral mounted over two 1–2 mm^2 hole in nitrocellulose filter paper (Millipore) with the photoreceptor layer side down, and stored in oxygenated Ames' media or ACSF until use (maximum 10 h). All experiments were performed on retinas in which dorsal-ventral orientation was tracked.

Visual Stimulation For visual stimulation of vDSGCs, broad-band visible light ranging from 470 to 620 nm was generated using an OLED display (SVGA Rev2 OLED-XL; eMagin) displaying custom stimuli created using MATLAB software with the Psychophysics Toolbox. Drifting bars were presented (velocity = 250 and 500 μm/s, length = 600 μm width = 350 μm over a 700 μm radius circular mask) in 8 block shuffled directions, repeated 3 times, with each presentation lasting 6 s and followed by 500 ms of gray screen) were projected through the 20X water-immersion objective (Olympus LUMPlanFl/IR 360/1.0 NA) onto the photoreceptor layer through the same 20x objective used to target cells once the cell attached recording configuration was achieved.

The directionally selective index (DSI) was calculated for spike responses as: (PD-ND)/(PD +ND) where PD is the number of spikes in the preferred direction and ND is the number of spikes in the null direction. We also used the magnitude of the vector sum of the spike responses as another measurement of directional tuning (Vector Sum = 1-Circular Variance of the spike responses, [Mazurek et al., 2014]).

Two-photon targeted loose patch and whole-cell voltage-clamp recordings Oriented retinas were placed under the microscope in oxygenated Ames' medium at 32–34°C. Identification and recordings from GFP+ cells were performed as described previously (Wei et al., 2010). In brief, GFP+ cells were identified using a custom-modified two-photon microscope (Fluoview 300; Olympus America) tuned to 920 nm to minimize bleaching of photoreceptors. The inner limiting membrane above the targeted cell was dissected using a glass electrode. Cell attached voltage clamp recordings were performed with a new glass electrode (4–5 MΩ) filled with internal solution containing the following (in mM): 110 CsMeSO4, 2.8 NaCl, 20 HEPES, 4 EGTA, 5 TEA-Cl, 4 Mg-ATP, 0.3 Na_3GTP, 10 Na_2Phosphocreatine, QX-Cl (pH = 7.2 with CsOH, osmolarity = 290, ECl^{-} = −60 mV). After cell attached recordings of spikes, whole cell recordings were performed with the same pipette after obtaining a GU seal. Holding voltages for measuring excitation and inhibition after correction for the liquid junction potential (−10 mV) were 0 mV and −60 mV, respectively. Signals were acquired using Clampex10.4 recording software and a Multiclamp 700A amplifier (Molecular Devices), sampled at 10 kHz, and low-pass filtered at 6 kHz. Current clamp recordings were performed with a new glass electrode (4–5 MU) filled with internal solution containing the following (in mM): 115 K^+ gluconate, 9.7 KCl, 1 $MgCl_2$, 0.5 $CaCl_2$, 1.5 EGTA, 10 HEPES, 4 ATP-Mg_2, 0.5 GTP-Na_3, 0.025, Alexa Fluor 594 (pH = 7.2 with KOH, osmolarity = 290). Tracer coupling experiments of GFP+ cells were performed as described previously (Caval-Holme et al., 2019).

Two-photon microscopy and morphological reconstruction After physiological recordings of vDSGCs were completed, Alexa-594-filled vDSGCs in the Hb9–GFP mice were imaged using the two-photon microscope at 700 nm. At this wavelength, GFP is not efficiently excited but Alexa 594 is brightly fluorescent. 600 × 600 μm Image stacks were acquired at z intervals of 1.0 μm and resampled fifteen times for each stack using a 20X objective (Olympus LUMPlanFl/IR 2x digital zoom, 1.0 NA) 30kHz resonance scanning mirrors covering the entire dendritic fields of the vDSGCs. Image stacks vDSGCs were then imported to FIJI (NIH) and a custom macro was used to segment ON and OFF dendrites based on their lamination depth in the inner plexiform layer (ON layer 10–30 μm, OFF layer 35–65 μm depth). Following ON and OFF dendritic segmentation, another custom FIJI macro uses the local maximum values of fluorescent pixels to binarize and skeletonize ON and OFF dendritic segments for morphological analyses.

Receptive field mapping To map excitatory and inhibitory receptive fields of vDSGCs, visual stimuli were generated using a computer running 420 nm light through a digital micro mirror device (DLI Cel5500) projector with a light emitting diode (LED) light source through a 20X objective (UMPlanFL 0.5NA W). Stimuli (30 μm^2) at an intensity of 4×10^9 photons/s/μm^2 were presented in a pseudorandom order, in a 10×10 grid, onto a stimulus

field of 500 μm^2, with the DSGC soma located in the center of the stimulus field (See Figure 5). Voltage clamp recordings were simultaneously acquired using methods described above.

Pharmacology—For experiments conducted in gabazine (Tocris, SR95531), we diluted 50 μM in AMES media, and allowed it to perfuse for 5–10 mins at a perfusion rate of 1 mL/min.

Retinal Histology—Whole-mount retinas were fixed in 4% PFA for 20 min, then washed in block solution (2% donkey serum, 2%bovine serum albumin, 0.3% Triton X-100 in PBS, 3 times, 16 min). Next, retinas were incubated in primary antibodies (1:1000 rabbit anti-GFP, Invitrogen, Grand Island, NY; 1:500 goat anti-ChAT, Millipore, Billerica, MA) for 1–3 days, and then washed in block solution (3 times, 15 min) and left in block solution at 4°C overnight. The retinas were then incubated in secondary antibody (1:1000 donkey anti-rabbit Alexa Fluor 488, 1:1000 donkey anti-goat Alexa Fluor 568; Invitrogen) at 4°C overnight. Then, they were washed in block solution (5 times, 30 min) and left in PBS overnight. Then, retinas were mounted and coverslipped with Vectashield (Vector Laboratories, Burlingame, CA).

Whole retina morphological analysis—Fixed and stained whole-mounted retinas were imaged on an epifluorescent macroscope (Olympus MV PLAPO 0.63x) within one week of mounting. Exposure and gain were adjusted per retina to maximize GFP signal. Images were then analyzed on FIJI for use in mosaic and nearest neighbor analysis (Figure S2). Whole retina fluorescent images were processed through a custom built MATLAB script and mosaic analysis was conducted on the imaged somas.

QUANTIFICATION AND STATISTICAL ANALYSIS

Statistical Tests—Details of statistical tests, number of replicates, and p values are indicated in the figures and figure captions. P-values less than 0.05 were considered significant.

Whole cell recordings—For cell attached vDSGC recordings, spike counts were calculated by bandpass filtering traces (0.08–2 kHz) and manually identifying a threshold value for spikes on the filtered traces. Local minima below threshold that did not violate refractory period criteria (0.001 s) were counted as spikes. ON and OFF responses were defined as spikes occurring within a 1.9 s time window starting right before the presentation of the leading or trailing edge of the stimulus. The average spike counts across the 3 trials were used to calculate the normalized vector sum of the spike responses. Preferred directions for both ON and OFF responses used to calculate average spike counts and were defined as the angle of the vector sum of spike responses for the ON and the OFF responses.

For voltage clamp recordings, traces were first average across the 3 trials for each direction and inspected to ensure consistency of responses. Average traces were baseline subtracted based on the last 500 ms of recording or a user defined interval after manual inspection. Peak currents were calculated from average baseline subtracted traces and were the maximal (IPSC) or minimal (EPSC) points during the 1.9 s window described above. The peak currents were used to calculate the vector sum of the current responses. Preferred directions

for both ON and OFF responses used to calculate peak responses and were defined as 180° - the angle of the vector sum of ON and OFF peak IPSCs, or the angle of the vector sum of ON and OFF peak EPSCs if IPSCs were not recorded in that cell.

For current clamp recordings, traces were first average across the 3 trials for each direction and inspected to ensure consistency of responses. Average traces were baseline subtracted based on the last 500 ms of recording or a user defined interval after manual inspection. Peak depolarizations were calculated from average baseline subtracted traces during the 1.9 s window described above. The peak depolarizations were used to calculate the vector sum of the current responses. Preferred directions for both ON and OFF responses used to calculate peak responses and were defined as the angle of the vector sum of ON and OFF peak EPSPs. All current clamp experiments were performed in the presence of 50 μM Gabazine.

Receptive field mapping—To quantify excitatory and inhibitory receptive field sizes for each cell, we first divided each trace into the ON and OFF response based on the stimulus we present. Next, we fit a two-dimensional Gaussian to the post synaptic current (PSC) peak values averaged over three trials. We use the 2x standard deviation of the Gaussian fit to display the size of the receptive fields.

To compare the size and location of the PSC receptive fields relative to the soma and to each other, we used the standard deviation and peak coordinates of the Gaussian fits, respectively.

Mosaic analysis—GFP+ somas were selected and a mask of the retinal outline was defined. vDSGC somas were manually marked for each retina to create binary masks, and boundaries of each whole mounted retina was manually traced. Using MATLAB, we generated a random array of binary points (equal to the number of somas for each retina) within the boundary mask of every retina. Next, we generated a custom MATLAB script to calculate the nearest neighbor distances (NND) of our masked somas, normalized to the total size of the retina, and compared these distances to the randomly distributed somas. The regularity index (or conformity ratio) was calculated by dividing the mean NND by the standard deviation from the mean (Wässle and Riemann, 1978). Both NND and regularity index metrics were compared to a random distribution of the same number of somas for each retina.

Single Cell morphological analysis—To calculate dendritic field size, the furthest dendritic extent was determined by adjusting brightness and contrast of individual maximum intensity z-projection images. A polygon was constructed using individual dendritic tips, and the area of the polygon is used as a measurement of dendritic field size.

To assess morphological alignment of vDSGC dendrites in oriented retinas, we calculated the center of mass of the dendritic pixels from the binarized vDSGC skeleton relative to the soma. Briefly, a FIJI macro was designed to do the following: 1) allow user to localize the soma, record soma coordinates, and then clear/exclude soma pixels from the stack and dendritic analysis 2) creates a maximum intensity projection of the dendritic pixels and measure their center of mass (COM) using the following equation:

$$\mathrm{COM_x} = \frac{\sum_{i=1}^{N} m_i x_i}{M}$$

$$COM_y = \frac{\sum_{i=1}^{N} m_i y_i}{M}$$

where N is the total number of image pixels, *x and y* are the coordinate distance of each pixel, M is the total number of dendritic pixels, and *m* is the mass of each pixel *i*, which is either 1 or 0. 3) Following COM calculation, the length of the vector from the dendritic COM to the soma coordinates is used as a measurement of dendritic asymmetry, and the angle of the vector from the dendritic COM to the soma coordinates is used as a measurement of dendritic angle.

Note: Dendritic reconstructions shown in figures were obtained by manually tracing example cells using the simple neurite tracer plugin on FIJI. Dendritic skeletons were then rendered and eroded for presentation.

Supplementary Material

Refer to Web version on PubMed Central for supplementary material.

ACKNOWLEDGMENTS

We thank Benjamin E. Smith for the dendritic analysis macro, Alex Tiriac and Mathew M. Summers for their contributions to the revision experiments, and members of the Feller lab for commenting on the manuscript. M.Q. was supported by the Ruth L. Kirschstein Pre-doctoral National Research Service Award from the NIH (F31 NS106756). K.M. was supported by the University of California (UC), Berkeley, Summer Undergraduate Research Fellowship (SURF). M.Q. and M.B.F. were supported by NIH grants R01EY019498, R01EY013528, and P30EY003176.

REFERENCES

Ackert JM, et al. (2009). GABA blockade unmasks an off response in on direction selective ganglion cells in the mammalian retina. Journal of Physiology 587 (18), 4481–4495. 10.1113/jphysiol.2009.173344. [PubMed: 19651763]

Arber S, Han B, Mendelsohn M, Smith M, Jessell TM, and Sockanathan S (1999). Requirement for the homeobox gene Hb9 in the consolidation of motor neuron identity. Neuron 23, 659–674. [PubMed: 10482234]

Bae JA, Mu S, Kim JS, Turner NL, Tartavull I, Kemnitz N, Jordan CS, Norton AD, Silversmith WM, Prentki R, et al.; Eyewirers (2018). Digital museum of retinal ganglion cells with dense anatomy and physiology. Cell 173, 1293–1306.e19. [PubMed: 29775596]

Balaskas N, Abbott LF, Jessell TM, and Ng D (2019). Positional strategies for connection specificity and synaptic organization in spinal sensory-motor circuits. Neuron 102, 1143–1156.e4. [PubMed: 31076274]

Barlow HB, and Levick WR (1965). The mechanism of cdirectionally selective units in rabbit's retina. J. Physiol 178, 477–504. [PubMed: 5827909]

Blanchart A, De Carlos JA, and López-Mascaraque L (2006). Time frame of mitral cell development in the mice olfactory bulb. J. Comp. Neurol 496, 529–543. [PubMed: 16572431]

Bos R, Gainer C, and Feller MB (2016). Role for visual experience in the development of direction-selective circuits. Current Biology, 1–9. 10.1016/j.cub.2016.03.073.

Briggman KL, Helmstaedter M, and Denk W (2011). Wiring specificity in the direction-selectivity circuit of the retina. Nature 471, 183–188. [PubMed: 21390125]

Caval-Holme F, Zhang Y, and Feller MB (2019). Gap junction coupling shapes the encoding of light in the developing retina. Curr. Biol 29, 4024–4035.e5. [PubMed: 31708397]

Choi JH, Law MY, Chien CB, Link BA, and Wong RO (2010). In vivo development of dendritic orientation in wild-type and mislocalized retinal ganglion cells. Neural Dev 5, 29. [PubMed: 21044295]

Demb JB (2007). Cellular mechanisms for direction selectivity in the retina. Neuron 55, 179–186. [PubMed: 17640521]

Ding H, Smith RG, Poleg-Polsky A, Diamond JS, and Briggman KL (2016). Species-specific wiring for direction selectivity in the mammalian retina. Nature 535, 105–110. [PubMed: 27350241]

Elias E, Yang N, Wang P, and Tian N (2018). Glutamate activity regulates and dendritic development of J-RGCs. Front. Cell. Neurosci 12, 249. [PubMed: 30154699]

Fried SI, Münch TA, and Werblin FS (2002). Mechanisms and circuitry underlying directional selectivity in the retina. Nature 420 (6914), 411–414. 10.1038/nature01179. [PubMed: 12459782]

Greenough WT, and Chang FLF (1988). Dendritic pattern formation involves both oriented regression and oriented growth in the barrels of mouse somatosensory cortex. Brain Res 471, 148–152. [PubMed: 3219592]

Hanson L, et al. (2019). Retinal direction selectivity in the absence of asymmetric starburst amacrine cell responses. eLife 8 10.7554/eL-ife.42392.

Harris RM, and Woolsey TA (1981). Dendritic plasticity in mouse barrel cortex following postnatal vibrissa follicle damage. J. Comp. Neurol 196, 357–376. [PubMed: 7217362]

Hinds JW, and Ruffett TL (1973). Mitral cell development in the mouse olfactory bulb: reorientation of the perikaryon and maturation of the axon initial segment. J. Comp. Neurol 151, 281–306. [PubMed: 4744475]

Hoon M, Okawa H, Della Santina L, and Wong ROL(2014). Functional architecture of the retina: Development and disease. Prog. Retin. Eye Res 42, 44–84. [PubMed: 24984227]

Kay JN, De la Huerta I, Kim IJ, Zhang Y, Yamagata M, Chu MW, Meister M, and Sanes JR (2011). Retinal ganglion cells with distinct directional preferences differ in molecular identity, structure, and central projections. J. Neurosci 31, 7753–7762. [PubMed: 21613488]

Kay JN, Chu MW, and Sanes JR (2012). MEGF10 and MEGF11 mediate homotypic interactions required for mosaic spacing of retinal neurons. Nature 483, 465–469. [PubMed: 22407321]

Kerschensteiner D, Morgan JL, Parker ED, Lewis RM, and Wong RO (2009). Neurotransmission selectively regulates synapse formation in parallel circuits in vivo. Nature 460, 1016–1020. [PubMed: 19693082]

Kostadinov D, and Sanes JR (2015). Protocadherin-dependent dendritic self- avoidance regulates neural connectivity and circuit function. eLife 4, e08964.

Lefebvre JL, Kostadinov D, Chen WV, Maniatis T, and Sanes JR (2012). Protocadherins mediate dendritic self-avoidance in the mammalian nervous system. Nature 488, 517–521. [PubMed: 22842903]

Lefebvre JL, Sanes JR, and Kay JN (2015). Development of dendritic form and function. Annu. Rev. Cell Dev. Biol 31, 741–777. [PubMed: 26422333]

Leighton AH, and Lohmann C (2016). The wiring of developing sensory circuits—from patterned spontaneous activity to synaptic plasticity mechanisms. Front. Neural Circuits 10, 71. [PubMed: 27656131]

Li H, Fertuzinhos S, Mohns E, Hnasko TS, Verhage M, Edwards R, Sestan N, and Crair MC (2013). Laminar and columnar development of barrel cortex relies on thalamocortical neurotransmission. Neuron 79, 970–986. [PubMed: 24012009]

Liu X, Grishanin RN, Tolwani RJ, Rentería RC, Xu B, Reichardt LF, and Copenhagen DR (2007). Brain-derived neurotrophic factor and TrkB modulate visual experience-dependent refinement of neuronal pathways in retina. J. Neurosci 27, 7256–7267. [PubMed: 17611278]

Matsui A, Tran M, Yoshida AC, Kikuchi SS, U M, Ogawa M, and Shimogori T (2013). BTBD3 controls dendrite orientation toward active axons in mammalian neocortex. Science 342, 1114–1118. [PubMed: 24179155]

Matsumoto A, Briggman KL, and Yonehara K (2019). Spatiotemporally asymmetric excitation supports mammalian retinal motion sensitivity. Curr. Biol 29, 3277–3288.e5. [PubMed: 31564498]

Mazurek M, Kager M, and Van Hooser SD (2014). Robust quantification of orientation selectivity and direction selectivity. Front. Neural Circuits 8, 92. [PubMed: 25147504]

Mizuno H, Luo W, Tarusawa E, Saito YM, Sato T, Yoshimura Y, Itohara S, and Iwasato T (2014). NMDAR-regulated dynamics of layer 4 neuronal dendrites during thalamocortical reorganization in neonates. Neuron 82, 365–379. [PubMed: 24685175]

Mizuno H, Ikezoe K, Nakazawa S, Sato T, Kitamura K, and Iwasato T (2018). Patchwork-type spontaneous activity in neonatal barrel cortex layer 4 transmitted via thalamocortical projections. Cell Rep 22, 123–135. [PubMed: 29298415]

Morrie RD, and Feller MB (2015). An asymmetric increase in inhibitory synapse number underlies the development of a direction selective circuit in the retina. J. Neurosci 35, 9281–9286. [PubMed: 26109653]

Morrie RD, and Feller MB (2018). A dense starburst plexus is critical for generating direction selectivity. Curr. Biol 28, 1204–1212.e5. [PubMed: 29606419]

Nakazawa S, Mizuno H, and Iwasato T (2018). Differential dynamics of cortical neuron dendritic trees revealed by long-term in vivo imaging in neonates. Nat. Commun 9, 3106. [PubMed: 30082783]

Narboux-Nême N, Evrard A, Ferezou I, Erzurumlu RS, Kaeser PS, Lainé J, Rossier J, Ropert N, Südhof TC, and Gaspar P (2012). Neurotransmitter release at the thalamocortical synapse instructs barrel formation but not axon patterning in the somatosensory cortex. J. Neurosci 32, 6183–6196. [PubMed: 22553025]

Pei Z, et al. (2015). Conditional Knock-Out of Vesicular GABA Transporter Gene from Starburst Amacrine Cells Reveals the Contributions of Multiple Synaptic Mechanisms Underlying Direction Selectivity in the Retina. The Journal of neuroscience : the official journal of the Society for Neuroscience 35 (38), 13219–32. 10.1523/JNEUROSCI.0933-15.2015. [PubMed: 26400950]

Peng YR, Tran NM, Krishnaswamy A, Kostadinov D, Martersteck EM, and Sanes JR (2017). Satb1 regulates contactin 5 to pattern dendrites of a mammalian retinal ganglion cell. Neuron 95, 869–883.e6. [PubMed: 28781169]

Pologruto TA, Sabatini BL, and Svoboda K (2003). ScanImage: flexible software for operating laser scanning microscopes. Biomed. Eng. Online 2, 13. [PubMed: 12801419]

Rall W (1964). Theoretical significance of dendritic trees for neuronal input output relations In Neural Theory and Modeling, Reiss RF, ed. (Stanford, CA: Stanford University Press), pp. 73–97.

Richards SEV, and Van Hooser SD (2018). Neural architecture: from cells to circuits. J. Neurophysiol 120, 854–866. [PubMed: 29766767]

Rivlin-Etzion, 2012Rivlin-Etzion M, Wei W, Feller MB, et al. (2012). Visual Stimulation Reverses the Directional Preference of Direction-Selective Retinal Ganglion Cells In Neuron (Elsevier Inc), pp. 518–525. 10.1016/j.neuron.2012.08.041.

Rockhill RL, Euler T, and Masland RH (2000). Spatial order within but not between types of retinal neurons. Proc. Natl. Acad. Sci. U S A 97, 2303–2307. [PubMed: 10688875]

Rosa JM, Morrie RD, Baertsch HC, and Feller MB (2016). Contributions of rod and cone pathways to retinal direction selectivity through development. J. Neurosci 36, 9683–9695. [PubMed: 27629718]

Sabbah S, Gemmer JA, Bhatia-Lin A, Manoff G, Castro G, Siegel JK, Jeffery N, and Berson DM (2017). A retinal code for motion along the gravitational and body axes. Nature 546, 492–497. [PubMed: 28607486]

Sivyer B, et al. (2010). Synaptic inputs and timing underlying the velocity tuning of direction-selective ganglion cells in rabbit retina. Journal of Physiology 588 (17), 3243–3253. 10.1113/jphysiol.2010.192716. [PubMed: 20624793]

Stuart GJ, and Spruston N (2015). Dendritic integration: 60 years of progress. Nat. Neurosci 18, 1713–1721. [PubMed: 26605882]

Sun LO, Jiang Z, Rivlin-Etzion M, Hand R, Brady CM, Matsuoka RL, Yau KW, Feller MB, and Kolodkin AL (2013). On and off retinal circuit assembly by divergent molecular mechanisms. Science 342, 1241974. [PubMed: 24179230]

Tian N, and Copenhagen DR (2001). Visual deprivation alters development of synaptic function in inner retina after eye opening. Neuron 32, 439–449. [PubMed: 11709155]

Trenholm S, Johnson K, Li X, Smith RG, and Awatramani GB (2011). Parallel mechanisms encode direction in the retina. Neuron 71, 683–694. [PubMed: 21867884]

Trenholm S, McLaughlin AJ, Schwab DJ, and Awatramani GB (2013). Dynamic tuning of electrical and chemical synaptic transmission in a network of motion coding retinal neurons. J. Neurosci 33, 14927–14938. [PubMed: 24027292]

Vaney DI, and Taylor WR (2002). Direction selectivity in the retina. Curr. Opin. Neurobiol 12, 405–410. [PubMed: 12139988]

Wässle H, and Riemann HJ (1978). The mosaic of nerve cells in the mammalian retina. Proc. R. Soc. London 200, 441–461. [PubMed: 26058]

Wei W, Elstrott J, and Feller MB (2010). Two-photon targeted recording of GFP-expressing neurons for light responses and live-cell imaging in the mouse retina. Nat. Protoc 5, 1347–1352. [PubMed: 20595962]

Wei W, Hamby AM, Zhou K, and Feller MB (2011). Development of asymmetric inhibition underlying direction selectivity in the retina. Nature 469, 402–406. [PubMed: 21131947]

Wong ROL, and Ghosh A (2002). Activity-dependent regulation of dendritic growth and patterning. Nat. Rev. Neurosci 3, 803–812. [PubMed: 12360324]

Woolsey TA, andVan der Loos H (1970). The structural organization of layer IV in the somatosensory region (SI) of mouse cerebral cortex. The description of a cortical field composedofdiscrete cytoarchitectonic units. Brain Res17, 205–242. [PubMed: 4904874]

Yao X, Cafaro J, McLaughlin AJ, Postma FR, Paul DL, Awatramani G, and Field GD (2018). Gap junctions contribute to differential light adaptation across direction-selective retinal ganglion cells. Neuron 100, 216–228.e6. [PubMed: 30220512]

Yonehara K, Balint K, Noda M, Nagel G, Bamberg E, and Roska B (2011). Spatially asymmetric reorganization of inhibition establishes a motion-sensitive circuit. Nature 469, 407–410. [PubMed: 21170022]

Yonehara K, Fiscella M, Drinnenberg A, Esposti F, Trenholm S, Krol J, Franke F, Scherf BG, Kusnyerik A, Müller J, et al. (2016). Congenital nystagmus gene FRMD7 is necessary for establishing a neuronal circuit asymmetry for direction selectivity. Neuron 89, 177–193. [PubMed: 26711119]

Zhang L, Wu Q, and Zhang Y (2020). Early visual motion experience shapes the gap junction connections among direction selective ganglion cells. PLoS Biol 18, e3000692. [PubMed: 32210427]

Highlights

- Visual deprivation prevents vDSGC dendrite orientation toward the ventral axis
- Ventral direction tuning is maintained despite altered dendritic orientation
- Inhibition-independent DS tuning is reduced in visually deprived vDSGCs
- Spatially offset, null direction inhibition is maintained in visually deprived vDSGCs

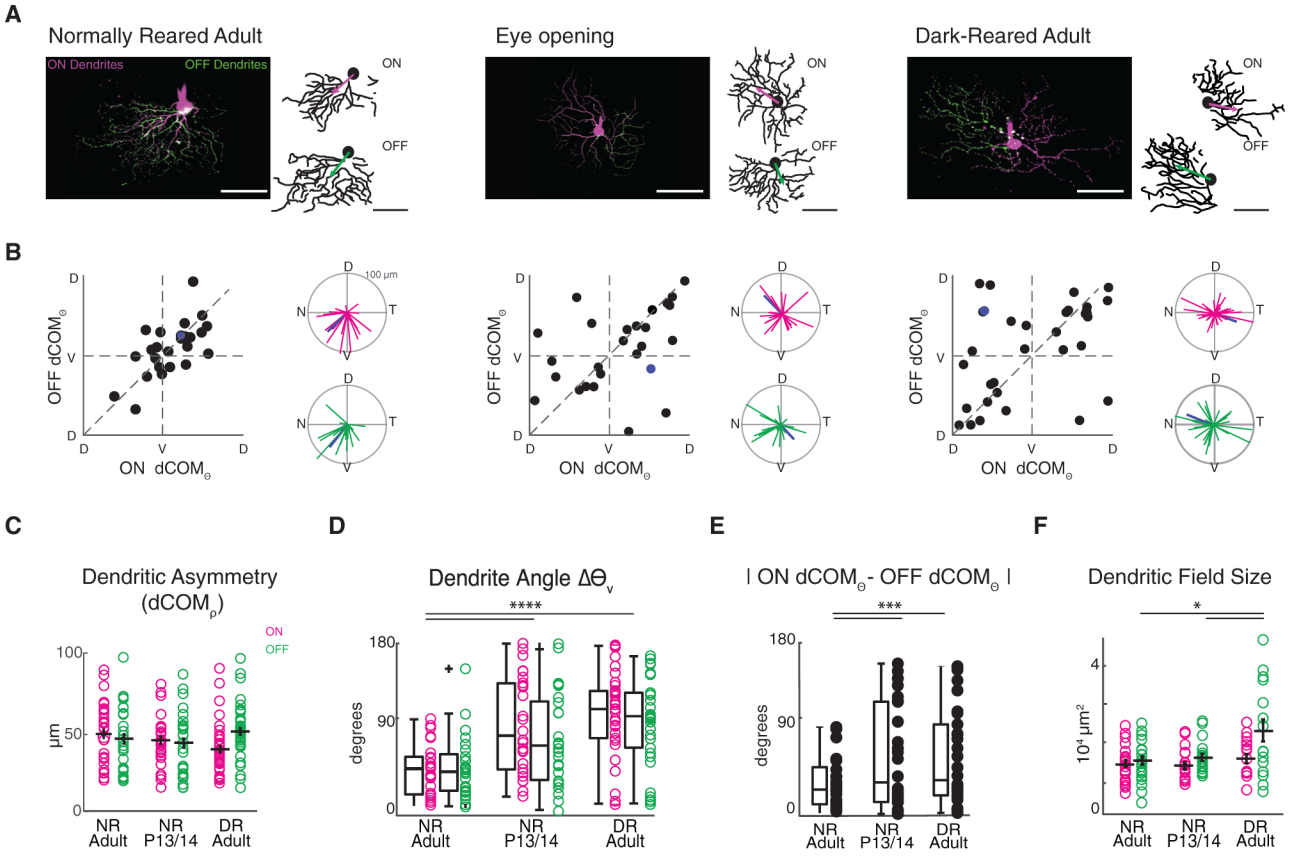

Figure 1. Dark-Rearing Prevents Orientation of vDSGC Dendrites toward the Ventral Direction

(A) Example maximum intensity projections (left) and binarized skeletons (right) of filled vDSGCs with ON (magenta) and OFF (green) dendrites segments for normally reared adults (left, P30–P50, NR adult), at eye opening (middle, NR P13/P14), and in adults that are dark-reared from birth (right, P30–P50, DR adult) with ON and OFF dCOM vectors overlaid on dendritic skeleton. Scale bar, 100 µm.

(B) Characterization of dendritic orientation in NR adults (n = 25 cells), at eye opening (n = 26 cells), and in DR adults (n = 35 cells). Left: ON versus OFF dendrite center of mass vector angle ($dCOM_\Theta$). Right: polar plots of ON (magenta) and OFF (green) dendrite center of mass vectors. Blue data points refer to example cell above.

(C) Summary data for dCOM vector magnitude as a measurement of ON (magenta) and OFF (green) dendritic asymmetry. Horizontal bar denotes mean; error bar denotes SEM. Significance was assessed using Kruskal-Wallis one-way ANOVA: p_{ON} and $p_{OFF} > 0.05$.

(D) Summary data for deviation of ON (magenta) and OFF (green) dendritic angle from the ventral (270°) axis for all three conditions. Horizontal bar denotes median. Boxplots represent variance. Kruskal-Wallis one-way ANOVA, Dunn-Siddak post hoc test: ****$p < 0.0001$.

(E) Summary data for absolute difference between ON (magenta) and OFF (green) dendritic angle. Horizontal bar denotes median. Boxplots represent variance. Significance was assessed using Levene's test for absolute variance: ***$p < 0.001$. (F) Summary data for ON and OFF dendritic field size of vDSGCs in three conditions. Horizontal bar denotes mean;

error bar denotes SEM. Significance was assessed using one-way ANOVA: $p = 8.7 \times 10^{-5}$; Tukey-Kramer post hoc test: *$p < 0.05$.

Mean ± SD values are presented in Table S1.

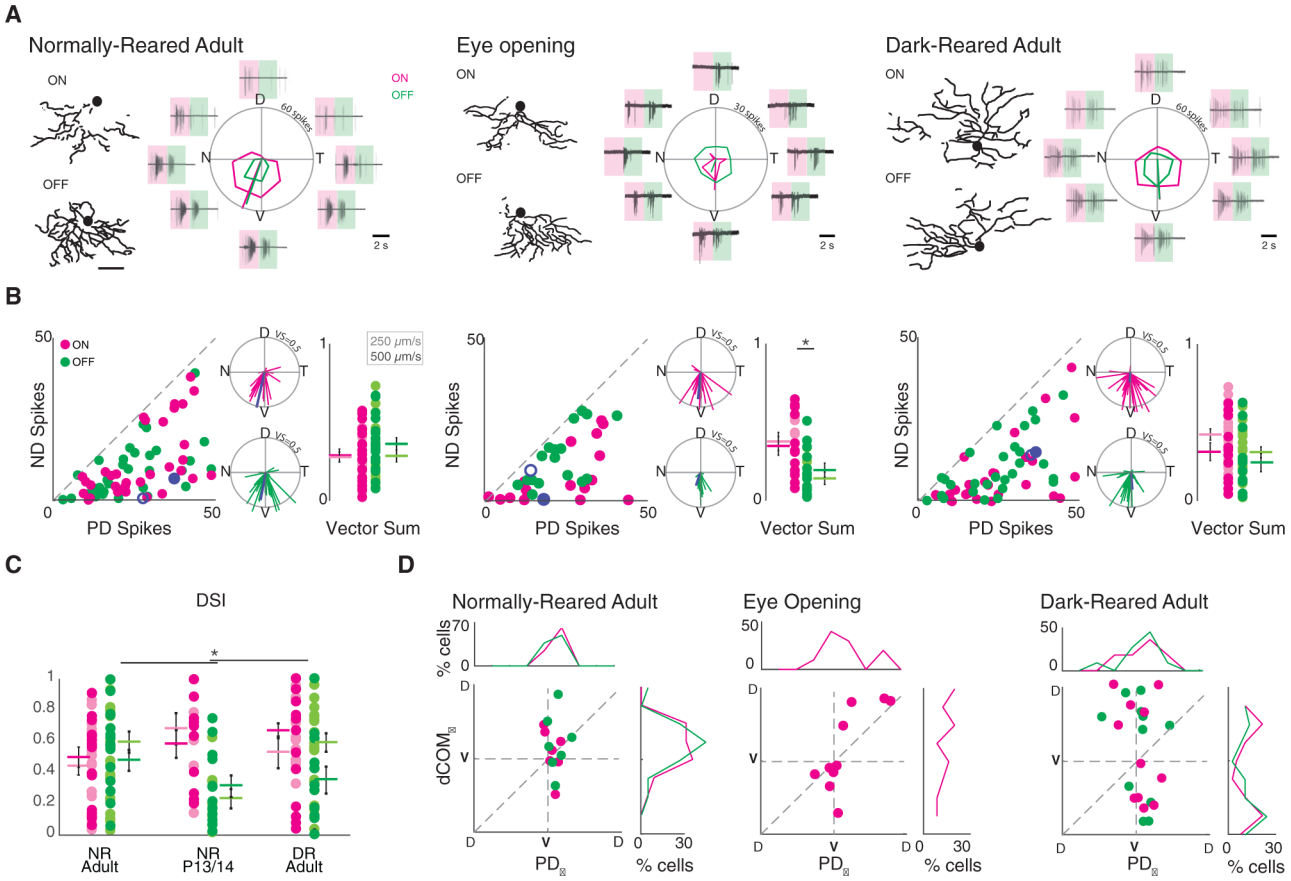

Figure 2. Ventral Motion Preference Is Preserved in Dark-Reared Mice Despite Altered vDSGC Dendritic Morphology

(A) Example dendritic skeletons of normally reared adult (left), eye opening (middle), and dark-reared adult (right) vDSGCs next to the average spike responses of the same cells. Shaded boxes define windows over which ON (magenta) and OFF (green) responses are assessed. Tuning curves plotted in polar coordinates ON (magenta) and OFF (green) responses. Radius of tuning curve = 60 spikes for adult and 30 spikes for eye opening. Scale bar = 100 μm.

(B) Population data represented as number of spikes fired for null direction (ND) versus preferred direction (PD) spiking (left) and as vectors in polar plots (middle inset) of normally reared adult (left, n = 39), eye opening (middle, n = 21), and dark-reared adult (right, n = 32) vDSGCs. Radius of polar plot: normalized vector sum (VS) of tuning curve = 0.5, blue data points refer to ON (filled) and OFF (open) responses of example cell above. Comparison of spike tuning using the magnitude of the normalized vector sum of the tuning curve (right inset) at two velocities (lighter shade, 250 μm/s; darker shade, 500 μm/s) for ON (magenta) and OFF (green) responses. Colored horizontal bar denotes mean; error bars denote SEM. Significance within conditions was assessed using unpaired t test: *$p_{250\mu m/s}$ = 0.005, $p_{500\mu m/s}$ = 0.05. Significance across conditions was assessed using one-way ANOVA for ON and OFF responses separately: p_{ON} = 0.08, p_{OFF} = 0.02. Tukey-Kramer post hoc test: $p > 0.05$.

(C) Comparison of spike tuning using direction selectivity index (DSI) at two velocities (lighter shade, 250 μm/s; darker shade, 500 μm/s) for ON (magenta) and OFF (green) responses. Colored horizontal bar denotes mean; error bars denote SEM. Significance was assessed using one-way ANOVA for ON and OFF responses separately: $p_{ON} = 0.11$, $p_{OFF} = 0.0022$. Tukey-Kramer post hoc test: $*p_{OFF}$ (NRadult-P13/P14) = 0.02.
(D) Comparison of dendritic orientation ($dCOM_{\Theta}$) versus spiking directional preference (PD_{Θ}), for normally reared adult (left, n = 12), eye opening (middle, n = 18), and dark-reared adult (right, n = 16) vDSGCs. X and y axes centered on ventral axis (V). Top inset: histogram illustrating vDSGC spiking angle. Right inset: histogram illustrating vDSGC dendritic orientation. Note that P13/P14 OFF responses were excluded from this analysis because of weak tuning (see Figure 2C). Mean ± SD values are presented in Table S2.

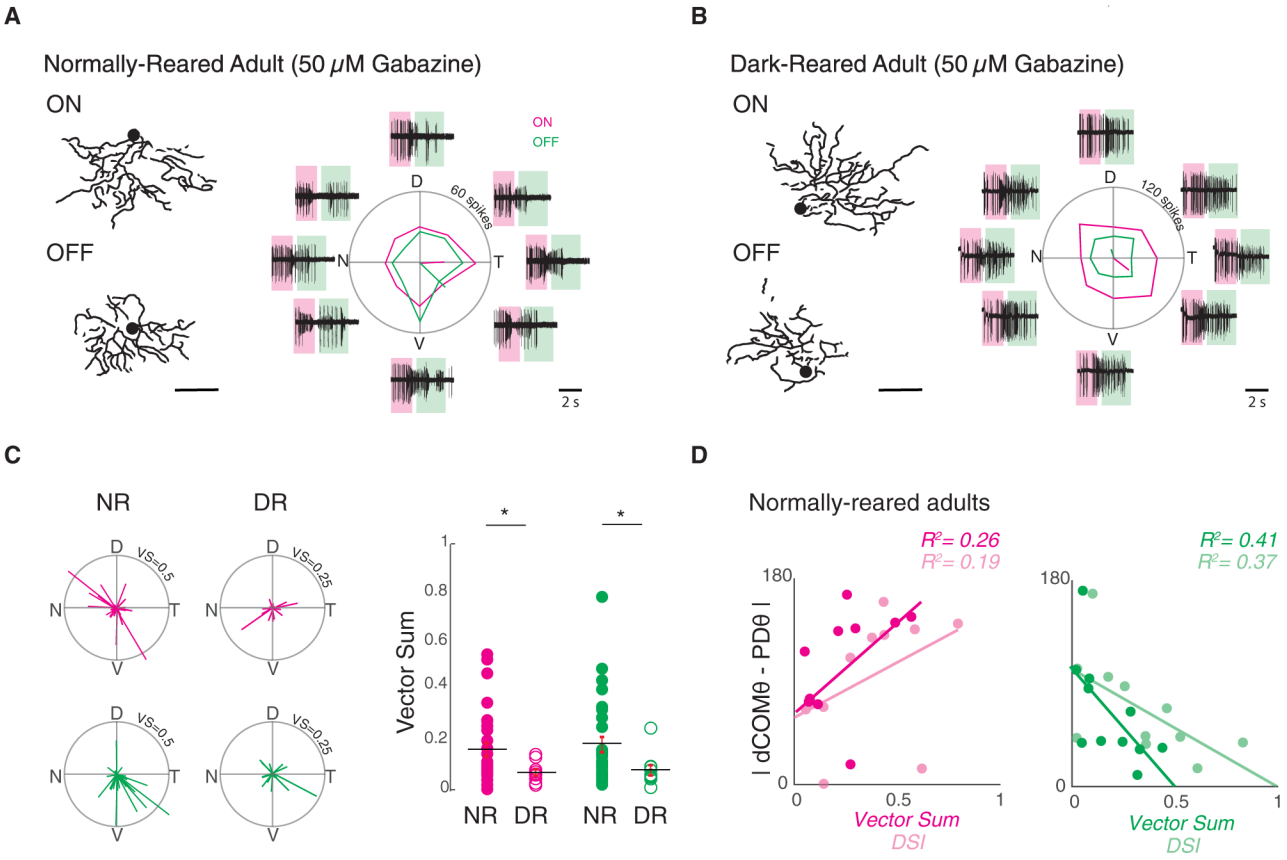

Figure 3. Inhibition-Independent Tuning Is Attenuated in Dark-Reared vDSGCs Because of Their Misoriented Dendrites

(A) Left: example dendrite skeletons for ON and OFF dendritic segments for normally reared adult vDSGCs. Scale bar, 100 μm. Right: example average spike responses of the same cell in the presence of 50 μM gabazine. Shaded boxes define windows over which ON and OFF responses are assessed. Tuning curves plotted in polar ON (magenta) and OFF (green) responses. Radius of tuning curve = 60 spikes.

(B) Left: example dendrite skeletons for ON and OFF dendritic segments for dark-reared adult vDSGCs. Right: example average spike responses of the same cell in the presence of 50 μM gabazine. Tuning curves plotted in polar ON (magenta) and OFF (green) responses. Radius of tuning curve = 120 spikes.

(C) Left: population data for normally reared (NR) adult vDSGC (left, n = 30) and dark-reared (DR) adult (right, n = 10) responses in 50 μM gabazine represented as vectors in polar plots. Data for ON (magenta) and OFF (green) plotted separately. Note that radius of polar plot is the normalized vector sum (VS) of the tuning curve = 0.50 (NR) and 0.25 (DR). Right: comparison of tuning strength as quantified by the magnitude of the normalized vector sum of the tuning curve in normally reared (NR; closed circles) and dark-reared (DR; open circles) adult vDSGCs across using a slow velocity stimulus (250 μm/s) in 50 μM gabazine. Data for ON (magenta) and OFF (green) plotted separately. Statistical significance was assessed across velocities using Wilcoxon rank-sum test. $p_{ON} = 0.03$, $p_{OFF} = 0.02$. *$p < 0.05$. Note that magnitude of vector sum of tuning curve is used here as a measure of tuning

strength, as we find that it better explains the variance between morphology-physiology alignment for both ON and OFF circuits. See Figure 3D and Figure S5C.

(D) Analysis of normally reared adult vDSGCs in 50 μM gabazine: how the strength of spike tuning measured by both the magnitude of the vector sum of the tuning curve (vector sum; darker shade) and direction selectivity index (DSI; lighter shade) varies with the degree of alignment of dendritic angle to the preferred direction of spiking. Data for ON (magenta) and OFF(green) plotted separately. R^2 value indicates fraction of the variance in tuning strength that is explained by morphology-physiology alignment and vice versa. Statistical significance of correlation coefficient was assessed using t test: $p_{ON} > 0.05$, $p_{OFF} < 0.05$. n = 10 cells.

Mean ± SD values are presented in Table S2.

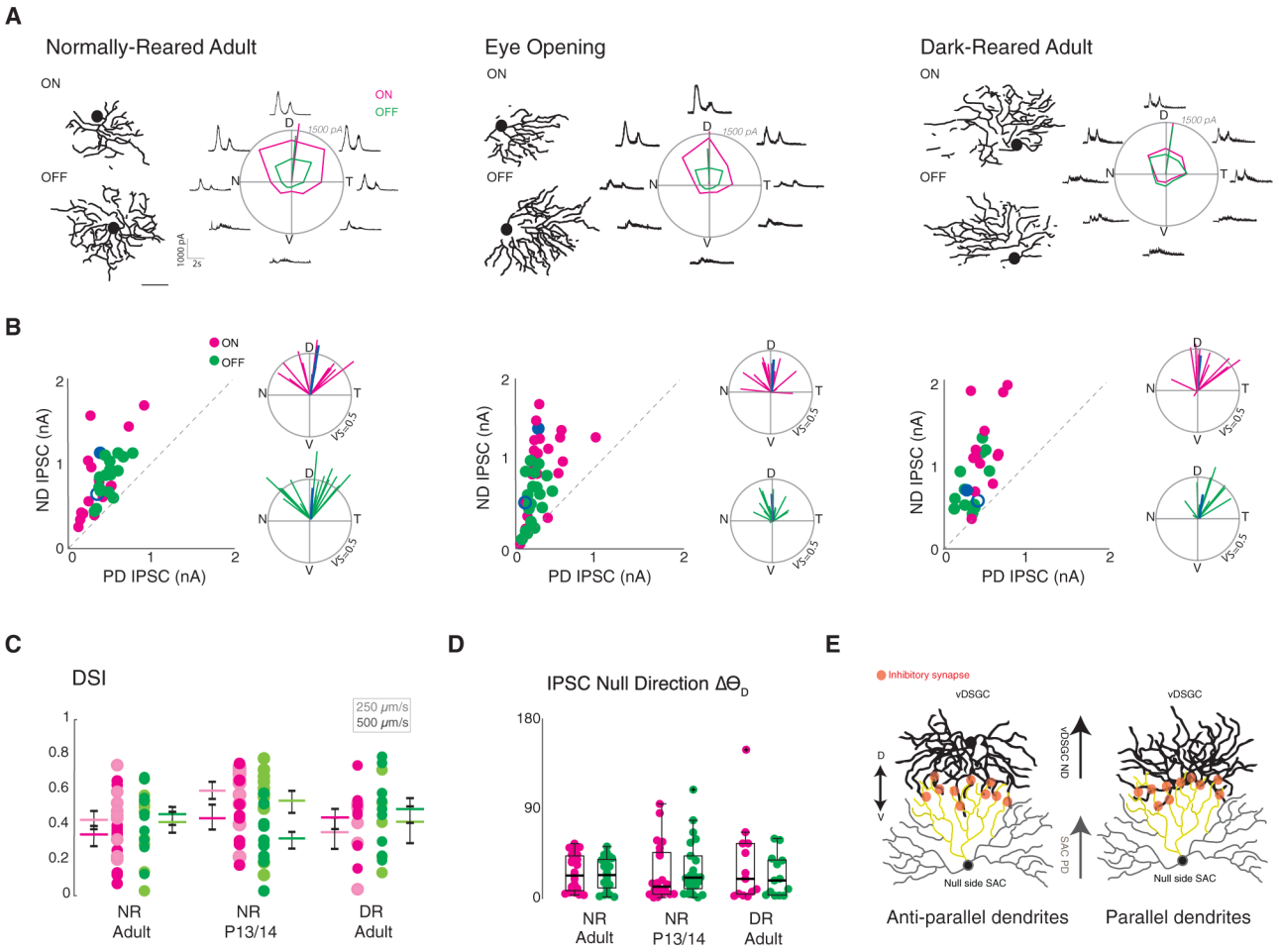

Figure 4. Asymmetric Inhibition Is Maintained in Dark-Reared vDSGCs

(A) Example dendritic skeletons of normally reared adult (left), eye opening (middle), and dark-reared adult (right) vDSGCs next to the average inhibitory currents of the same cells. Tuning curves plotted in polar coordinates ON (magenta) and OFF (green) responses. Radius of tuning curve = 1,500 pA. Scale bar = 100 μm.

(B) Left inset: population data for normally reared adult (left, n = 23), eye opening (middle, n = 22), and dark-reared adult (right, n = 13) vDSGCs represented as peak amplitude of inhibitory postsynaptic current (IPSC) recorded for null direction (ND) versus preferred direction (PD) stimulation. Right inset: polar plot for normalized vector sums of population IPSC tuning curves. Radius of polar plot: vector sum of tuning curve = 0.5. Blue data points refer to ON (filled) and OFF (open) example cell above.

(C) Tuning strength vDSGC inhibitory input, across two stimulus velocities (lighter shade, 250 μm/s; darker shade, 500 μm/s) quantified as the direction selectivity index (DSI) for normally reared (NR) adult, eye opening (NR P13/P14), and dark-reared (DR) adult. Colored horizontal bar denotes mean; error bars denote SEM. Statistical significance was assessed using one-way ANOVA: $p > 0.05$.

(D) Summary data for deviation of preferred direction of IPSC tuning of vDSGCs (ND) from the dorsal (90°) axis for all three conditions. Horizontal bar denotes median. Boxplots represent variance. Kruskal-Wallis test: $p > 0.05$. (E) Antiparallel SAC-vDSGC wiring

(Briggman et al., 2011), whereby vDSGCs preferentially synapse with null side SACs such that SAC preferred direction (PD) is aligned with vDSGC null direction (ND), schematized under two dendritic geometries. Left: vDSGCs with ventrally oriented dendrites synapse with null-side SACs where dendrites are oriented antiparallel to each other, right: vDSGCs with misoriented dendrites synapse with null-side SACs where dendrites are oriented parallel to each other.

Mean ± SD values are presented in Table S3.

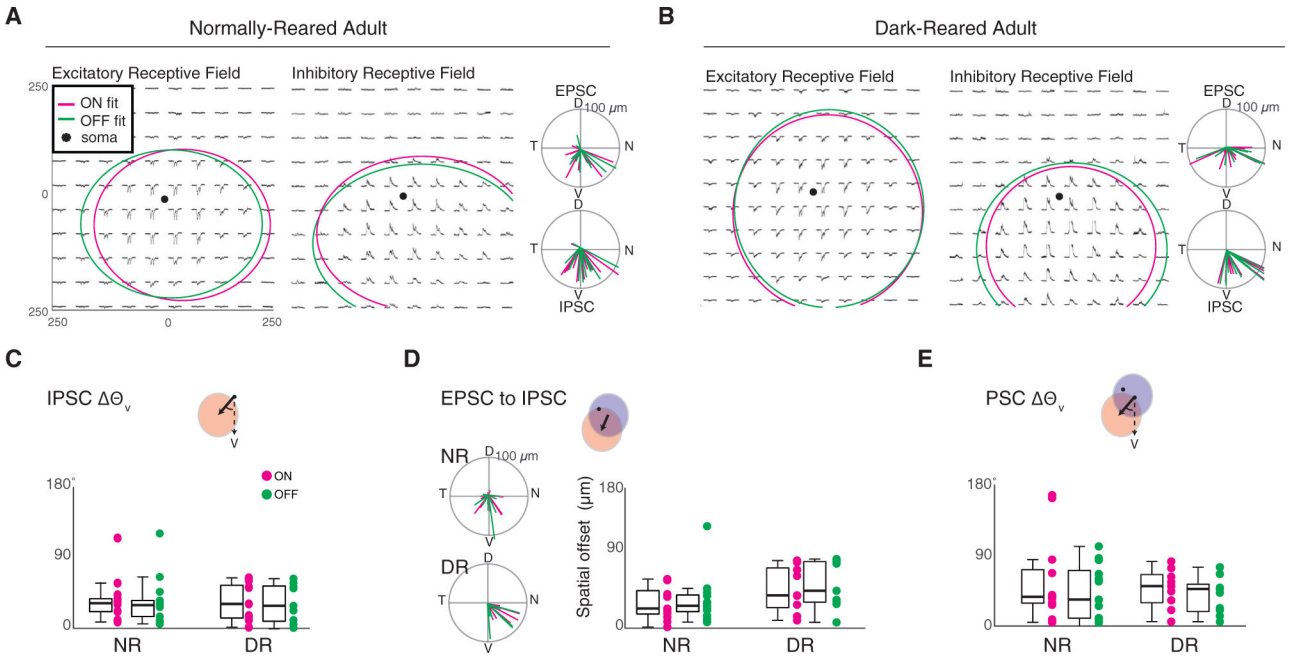

Figure 5. The Inhibitory Receptive Field Is Spatially Offset from the Excitatory Receptive Field in Adult vDSGCs

(A and B Example mean excitatory (left) and inhibitory (right) PSC responses of normally reared (A) and dark-reared adult

(B) vDSGCs. Peak amplitude of ON (magenta) and OFF (green) responses are fit with a 2-dimensional Gaussian. Ellipse radius in x and y axes = 2 SDs of the Gaussian fit centered on fit peak. Right: population data of NR adult vDSGCs represented as polar plots of vectors from the soma to the excitatory (top) and inhibitory (bottom) receptive field fits. Radius of polar plot = 100 μm, center of polar plot = soma location. NR, n = 13; DR, n = 9.

(C) Comparison of the orientation of the vector from the soma to the center of the inhibitory receptive field, relative to the ventral axis (ΔΘv). One-way ANOVA: $p > 0.05$.

(D) Left: population data of NR (top) and DR (bottom) adult vDSGCs represented as polar plots of vectors from the excitatory to the inhibitory receptive field centers. Radius of polar plot = 100 μm, center of polar plot = EPSC receptive field center. Right: comparison of the spatial offset (the magnitude of the vector) from the center ON (magenta) and OFF (green) excitatory receptive field to the center of the ON and OFF inhibitory receptive field fits (indicated in schematic above, where excitatory receptive field fit is in blue and inhibitory receptive field fit is in red) in NR and DR adult vDSGCs. One-way ANOVA: $p > 0.05$.

(E) Comparison of the orientation of the vector from the center of the excitatory receptive field to the center of the inhibitory receptive field, relative to the ventral axis (ΔΘv). Statistical significance was assessed using one-way ANOVA: $p > 0.05$.

Mean ± SD values are presented in Table S3.

KEY RESOURCES TABLE

REAGENT OR RESOURCE	SOURCE	IDENTIFIER
Antibodies		
Rabbit polyclonal anti-GFP	Invitrogen	Cat#A-11122; RRID: AB_221569
Goat polyclonal anti-Choline Acetyltransferase (ChAT)	Millipore	Cat#AB144P; RRID:AB_2079751
Donkey anti-rabbit Alexa Fluor 488	Invitrogen	Cat#A-21206; RRID:AB_2535792
Donkey anti-goat Alexa Fluor 594	Invitrogen	Cat# A-11058; RRID:AB_2534105
Chemicals, Peptides and Recombinant proteins		
Vectashield	Vector Laboratories	Cat# H-1400; RRID: AB_2336787
Neurobiotin	Vector Laboratories	Cat# SP-1120; RRID: AB_2313575
Streptavidin Alexa Fluor 594 conjugate	Invitrogen	Cat# S11227; RRID:AB_2337250
QX 314 Chloride	Tocris	Cat# 2313
Ames' Media	Sigma	Cat# A1420–10X1L
SR 95531 hydrobromide (gabazine)	Tocris	Cat# 1262
Experimental Models: Organisms/Strains		
Mouse: B6.Cg-Tg(Hlxb9-GFP)1Tmj/J (Hb9:GFP)	The Jackson Laboratory	RRID: IMST_JAX:005029
Software and Algorithms		
Simple Neurite Tracer FIJI plugin	NIH	https://imagej.net/SNT
FIJI	NIH	https://imagej.nih.gov/ij; RRID:SCR_003070
MATLAB	Mathworks	https://www.mathworks.com/products/matlab.html;; RRID: SCR_001622
FIJI Dendrite analysis macro	This paper	
ScanImage4	(Pologruto et al., 2003)	http://scanimage.vidriotechnologies.com/display/SIH/ScanImage+Home; RRID: SCFL014307
Clampex 10.3	Molecular Devices	RRID: SCR_011323